Progress In Electromagnetics Research B, Vol. 46, 23–40, 2013

HYBRID MULTI-PHASED PARTICLE SWARM OPTIMIZATION FOR THROUGH-WALL SHAPE RECONSTRUCTION AND WALL PARAMETERS ESTIMATION

Jiliang Cai[1, *], Chuangming Tong[1, 2], and Weijie Ji[1]

[1]Missile Institute, Air Force Engineering University, Xi'an, Shanxi 710051, China

[2]State Key Laboratories of Millimeter Waves, Nanjing, Jiangsu 210096, China

Abstract—When particle swarm optimization (PSO) technique is used for the inverse scattering problems it will take unbearably long time for the final solution, especially when the PSO algorithm traps into the premature convergence. To overcome this problem a hybrid multi-phased particle swarm optimization algorithm (HMPPSO) is proposed. By adopting the small swarm size strategy and the idea of "sub swarms" working cooperatively and alternatively with "optimal swarm" into the MPPSO, the HMPPSO can converge quickly with much less fitness function evaluation times, thus will reduce the reconstruction time. After the HMPPSO is validated by the numerical simulations on benchmark functions, the wall parameters (permittivity, conductivity, and thickness) together with target shape parameters (approximated by the trigonometric serials) with 20 dB additive Gaussian white noise are successfully reconstructed by HMPPSO using multi-frequency, multiview/singleillumination scattering fields calculated by MOM.

1. INTRODUCTION

Detection of targets behind the wall by electromagnetic wave is of increasing importance when the entering of a room or a building is considered to be hazardous or impossible in a wide range of both civilian and military applications such as calamity rescue, urban-warfare, and counterterrorism A number of research works focusing on this topic are reported in [1, 2].

Received 10 September 2012, Accepted 5 November 2012, Scheduled 13 November 2012

* Corresponding author: Jiliang Cai (shitouji840716@126.com).

Generally, to discern the target shape is one subject of the inverse scattering problem and methods such as Born approximation (BA) [3], contrast source inversion (CSI) [4], subspace-based optimization (SOM) [5] and multiple signal classification (MUSIC) [6] are developed. But the most seen method is by casting it into a constrained optimization problem [7–15]. While the error between the measured scattering coefficient and the computed scattering coefficient is considered as the cost function, the shape parameters of the target are viewed as the variables to be optimized and the corresponding electromagnetic equations are as the constraints. There are two types of methods to solve the constrained optimization problems. One is deterministic method based on the gradient, including Newton Kantrovitch method (NK) [7], Conjugate Gradient (CG) [8], Levenberg Marquardt (LM) [9]. Such methods are local optimization in essence and can find the local minimum quickly. However, they are not robust at least on the two aspects: firstly, to find the global minima for multi-optima problems, a proper guess of initial solution are needed, but usually it is difficult; secondly, the first and the second order of gradient of the cost function are needed, which will lead to large amount of computation. The other is based on stochastic methods, including particle swarm optimization (PSO) [10], genetic algorithm (GA) [11], differential evolution (DE) [12] and ant colony optimization (ACO) [13] etc., which can find the global without initial guess of the solution or the gradient information about the cost function.

One of the main advantages of PSO over the other stochastic optimization methods such as GA, ACO, DE and so on, lies in its ease of implementation, using only a velocity operator to drive the search throughout the hyperspace [14]. And it has been applied to the microwave image problems successfully [15–20]. However, like other stochastic algorithms, PSO also suffers from trapping into local optimal minimum and this may lead to the premature convergence. When this happens, all particles gather around it, and huge number of fitness function evaluation times are needed to encourage a global search, which would lead to unbearable computation time.

Many techniques have been proposed to avoid the premature convergence of PSO [15, 21–23]. They do improve the global searching ability to some extent, but are hard to get a good tradeoff between the global searching ability and the convergent efficiency. In their experiments on benchmark testing functions, hundreds of thousands of fitness function evaluation times are needed to get a satisfying solution. As is known, when PSO is applied to solve inverse scattering problems, one fitness function evaluation corresponds to a single forward scattering problem solution. Since the scattering forward

problem is time-consuming itself, too many fitness function evaluation times for the final inverse scattering solution will take unbearably long time. To save the computation time, the number of fitness function evaluation times must be reduced. Therefore, it is wise to adopt the small swarm size strategy as well as quick convergence searching mechanism. In [15], Huang proposed a micro PSO, in which there are only 3 or 5 particles in the swarm, to retrieve the dielectric coefficient of non-homogeneous dielectric objects.

With the multi-phase mechanism, multi-phase PSO (MPPSO) proposed in [21, 22] can guarantee the convergence rate and the precision of the solution, but there is still room to be improved. In order to improve the global searching ability of MPPSO with small swarms, in this paper, a hybrid MPPSO (HMPPSO) is proposed for through-wall shape reconstruction and wall parameters estimation. To achieve a good balance between the global searching ability and the convergent efficiency, the swarms are divided into several small groups, which are called sub swarms. The global best particle of each sub swarm is used to form an optimal swarm. Their sizes are all kept small and they work cooperatively and alternatively following the MPPSO updating rules. To improve the searching ability, the reinitiating operator and the feedback operator are also introduced. Numerical simulation results on some benchmarks show that comparing with SPSO and MPPSO, HMPPSO is more effective and robust. Then the HMPPSO is used for through-wall shape reconstruction and wall parameters estimation.

The remaining sections of this paper are organized as follows: Section 2 states the forward problem and the formulation of scattered field from a 2-D metallic cylinder behind the wall. Section 3 describes the proposed HMPPSO and its validation on benchmark functions. Numerical results for several targets of different shape behind the wall are given in Section 4. Section 5 is the conclusion.

2. FORWARD PROBLEMS [12]

Figure 1 shows the geometry of the through wall inverse scattering problem. An electric line source placed at $(-x_A, 0)$ before a solid wall radiates TM polarization of incident field. A hidden metallic cylinder with the cross section of any shape is placed at $(x_S, 0)$ behind the wall. The measurement points are symmetrically posited at $(-x_A, y_n)$ along a line parallel to the wall. The scattered fields from the cylinder are measured at different frequencies f_m and positions $y = y_n$.

Here, we assume that the source/observation points are relatively far from the target so that the incident fields on the target and

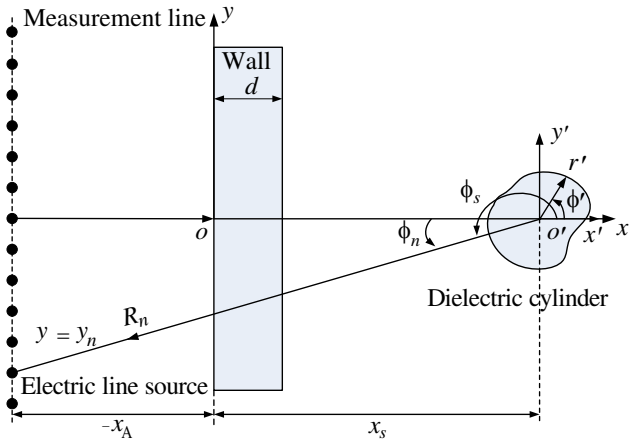

Figure 1. Through wall geometry of the inverse scattering problem.

scattered fields measured at the observation points are approximately plane waves. Besides, if the target and the measurement points are far enough from the wall, then the wall reflection is mainly the specular one and the target and wall multiple scattering can be ignored. Assuming $e^{-j\omega t}$ time convention, the scattered electric field E_r^z at the observation point y_n is approximately:

$$E_z^r(y_n, k_m) \approx \tau(d, \epsilon_r, \phi_i = 0, k_m) \cdot \tau(d, \epsilon_r, \phi_n, k_m) P\left(r'\left(\phi'\right), \phi_n, k_m\right) \times \frac{e^{2ik_m R_n}}{R_n} + \gamma(d, \epsilon_r, \phi_i = 0, k_m) \frac{e^{2ik_m |x_A|}}{\sqrt{|x_A|}} \tag{1}$$

where k_m is the wave number at frequency f_m, R_n is the distance between the antenna and the target center (i.e., the O'). The 2-D scatter field of the target is denoted by $P\left(r'(\phi'), \phi_n, k_m\right)$, where $\phi_n = -\arcsin(y_n/R_n)$ and $R_n = \sqrt{(x_S - x_A)^2 + y_n^2}$, $r'(\phi')$ is the shape of the cylinder. For a TM polarization incident field, the wall transmission coefficients $\tau\left(d, \epsilon_r, \phi_n, k_m\right)$ and the wall reflection coefficient at normal incidence $\gamma\left(d, \epsilon_r, \phi_i = 0, k_m\right)$ are given as:

$$\tau = \frac{4e^{i(k_{1x} - k_{0x})d}}{(1 + P_{01})(1 + P_{10})(1 + R_{01}R_{10}e^{2ik_{1x}d})} \tag{2}$$

$$\gamma = \frac{R_{01} + R_{10}e^{2ik_{1x}d}}{(1 + R_{01}R_{10}e^{2ik_{1x}d})} \tag{3}$$

where $R_{10} = -R_{01} = (1 - p_{10})/(1 + p_{10})$, $p_{10} = 1/p_{01}$, $p_{10} = k_{0x}/k_{1x}$, d is the thickness of the wall, and k_{0x} and k_{1x} are the normal components

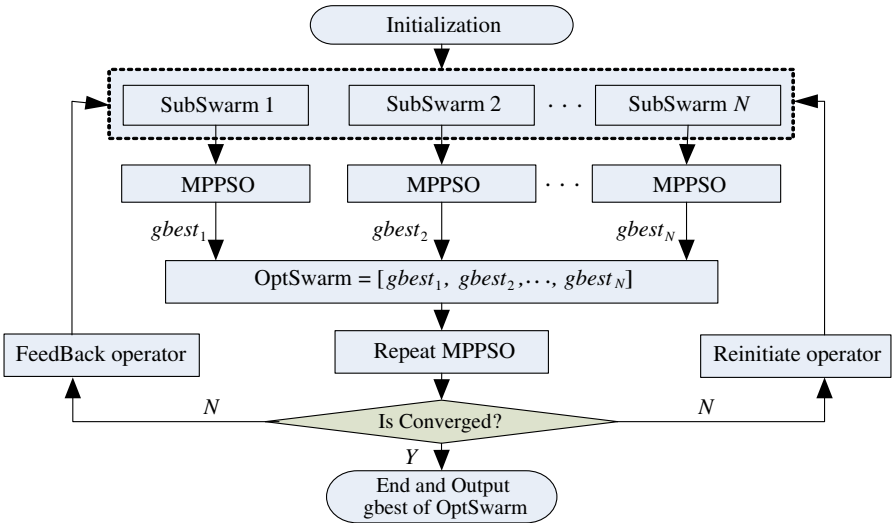

Figure 2. The flowchart of HMPPSO.

of the propagation constants in the air and in the dielectric wall, respectively.

To calculate $P\left(r'(\phi'),\, \phi_n,\, k_m\right)$, the method of moment is used. The electric current $\mathbf{J}$ satisfying the boundary condition is given by:

$$e^{ik_m r\cos(\phi-\phi_n)} = \frac{k_m Z_0}{4}\oint_C J\left(\phi'\right) H_0^1\left(k_m\left\|\mathbf{r}-\mathbf{r}'\right\|\right) r' d\phi' \tag{4}$$

where $\|\mathbf{r}-\mathbf{r}'\| = \sqrt{r^2+r'^2-2rr'\cos(\phi-\phi')}$, Z_0 is the free-space intrinsic impedance. $H_0^1(\cdot)$ is the Hankel function of first kind and zeroth order, r and ϕ denote polar coordinates of points on the target boundary.

After $\mathbf{J}$ is solved by Equation (4), the 2-D scattering of the isolated metallic cylinder observed along ϕ_s is given by:

$$P\left(r'\left(\phi'\right),\phi_s,k_m\right) = -Z_0\sqrt{\frac{k_m}{8i\pi}}\oint_C J\left(\phi'\right) e^{-ik_m r\cos(\phi_s-\phi')} r' d\phi' \tag{5}$$

It is noted that for scattering computation in (5), ϕ_s is set to $\pi+\phi_n$.

3. INVERSE PROBLEM

The inverse scattering problem is now to find the target shape $r'(\phi')$, and the wall parameters (i.e., wall thickness d the wall conductivity σ and the wall relative dielectric permittivity ϵ_r) using scattered fields

measured at positions y_n and frequency points f_m. In the following, the target shape representation and the HMPPSO to solve the inverse scattering problem are addressed.

3.1. Target Shape Representation

The cylinder shape $r'(\phi')$ represented by trigonometric series is as follow [11]:

$$r'\left(\phi'\right) = \sum\nolimits_{n=0}^{N} \left[a_n \cos\left(n\phi'\right) + b_n \sin\left(n\phi'\right)\right] \tag{6}$$

where ϕ' is the polar angle, and a_n and b_n are the coefficients to be reconstructed. Once they are known, the shape can be obtained. Generally, the bigger N is, the finer $r'(\phi')$ approaches the true shape, and for most of the occasions, $N = 3$ is enough for shape reconstruction.

3.2. Through-wall Shape Reconstruction and Wall Parameters Estimation

Since the shape is represented by trigonometric series, for through-wall shape reconstruction and wall parameters estimation, there are 10 parameters to be estimated by HMPPSO. Like other population based optimization methods, firstly, a random population of N_v parameter vectors $\mathbf{X}_i$ ($i \in \{1, 2, 3, \ldots, N_v\}$) is generated. Each random vector $\mathbf{X}_i$ consists of ten random elements: seven trigonometric series shape control parameters: a_0^i, a_1^i, a_2^i, a_3^i, b_1^i, b_2^i, b_3^i, three wall parameters: d^i, σ^i, ϵ_r^i. That is:

$$\mathbf{X}_i = \left[a_0^i, a_1^i, a_2^i, a_3^i, b_1^i, b_2^i, b_3^i, d^i, \sigma^i, \epsilon_r^i\right] \tag{7}$$

The elements of $\mathbf{X}_i$ are initialized and then updated yielding to a smaller cost function value with iterations by HMPPSO. Here, the cost function is defined as:

$$C\left(\mathbf{X}_i\right) = \frac{\sum_{m=1}^{N_f} \sum_{n=1}^{N_y} \left|E_{meas}^r\left(y_n, k_m\right) - E_{iter}^r\left(y_n, k_m, \mathbf{X}_i\right)\right|^2}{\sum_{m=1}^{N_f} \sum_{n=1}^{N_y} \left|E_{meas}^r\left(y_n, k_m\right)\right|^2} \tag{8}$$

where the subscripts *meas* and *iter* stand for measured and iterative values of scattering fields, respectively. Using (1), the measured scattering fields are calculated assuming the true parameters are known and the iterative ones are calculated with the current parameters of $\mathbf{X}_i$. In (8), N_f and N_y are the number of frequencies and observation points, respectively.

When termination criteria meets, the search of HMPPSO is stopped and the global best particle corresponds to the parameters to be reconstructed.

4. THE HYBRID MPPSO (HMPPSO)

4.1. Multi-phase PSO (MPPSO)

MPPSO, a developed version of PSO by Buthainah in [21, 22], introduces the concepts of 'group' and 'phase', which are defined as follows: when the fitness of the particle does not change any more, the particle's flying speed and direction in the searching space will change by the adaptive velocity strategy. Compared with standard PSO, MPPSO has three different characteristics: (1) dividing particles into multiple groups to increase the diversity of the swarm and extensiveness of the exploration space; (2) introducing different phases that have different flying directions and searching ways; and (3) generally speaking, the search is only along the direction that will decrease fitness.

The tentative particle velocity and position updating equations of the MPPSO are presented as follows:

$$V_i(k+1) = C_v \cdot V_i(k) + C_x \cdot X_i(k) + C_g \cdot gbest(k) \quad (9)$$

$$X_i(k+1) = X_i(k) + V_i(k+1) \quad (10)$$

where the C_v, C_x, C_g are the coefficients in each group within each phase. The details of the parameters are available in Ref. [22].

By using multi phase technology, the searching trajectories are disturbed randomly and cover most of the solution space. What is more, at the prophase of the evolution, each particle flies to the best position while at the anaphase, when every particle comes close to the global optimal, the searching trajectories are intercrossed and all the particles search intensively around the global minimum due to the effect of multi phase. These guarantee the convergence rate and the precision of the solution.

4.2. The Hybrid MPPSO (HMPPSO)

As described above, multi phase technology is used in MPPSO to guarantee the convergence rate and the precision of the solution; however, to make a good tradeoff between global searching and local exploration, still there is room to be improved. When it comes to the end of the optimization, the swarm loses diversity, and is trapped into the local minimum. This can be seen from the simulation results in Figs. 3, 4.

To improve the searching ability, especially at the anaphase, a hybrid MPPSO with sub swarms, called HMPPSO, is developed. The strategy used in MPPSO is described as follows:

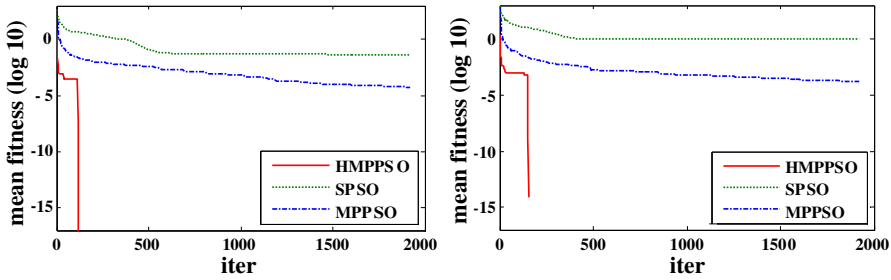

Figure 3. Dynamic performance comparison on the Griewank function. (a) $N = 30$, (b) $N = 50$.

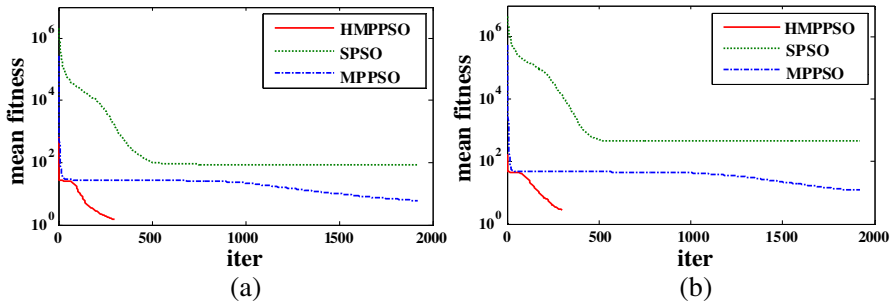

Figure 4. Dynamic performance comparison on the Rosenbrock function. (a) $N = 30$, (b) $N = 50$.

1. The sub swarms and the optimal swarm working cooperatively and alternatively: to achieve extensive global searching, the swarm is divided into many sub swarms. All of them are the same size and they search independently following MPPSO updating rules to generate the optimal swarm, which is made up by the *gbest* particle of each sub swarm. When the optimal swarm finishes its updating by MPPSO rules, the feedback operator, by which the *gbest particle* and a random selected particle of the **i-th** sub swarm are substituted by the **i-th** particle's current best position of the optimal swarm, starts to enhance the information exchange between each sub swarm and the optimal swarm. Since MPPSO converges quickly at prophase, the sub swarms and optimal just iterate several times rather than hundreds of times. What is more, too much iteration will lead to frequent velocity reinitiating, which is not beneficial for searching.

2. Optimal swarm working repeatedly: to achieve intensive local

exploration, the optimal swarm repeated searching several times for the current best positions and the *gbest* particle which will feedback to the sub swarms to guide them flying to the global optimal. After repeating three to five times, the optimal swarm will concentrate in a very small zone, therefore, more repeating will be a waste of computation.

3. The Reinitiate operator: to maintain the variety of the swarm, when the optimal swarm finishes, all the sub swarms' velocity is reinitiated and this will help to escape from the local minima

4. Small swarm size: to reduce the number of fitness function evaluation times and the computation time, in [15], a micro MPPSO is developed to solve high-dimensional problems. In this paper, all the swarms' sizes are kept small too. Generally, 2 to 5 particles in each sub swarm and 8–15 sub swarms is enough.

5. Soft boundary control: if any dim of a particle's velocity or position is out of the boundary, it will be replaced by a random number in the scope generated by *boundary*rand(0, 1)*, rather than just is instead by *boundary* in hard boundary control.

For better understanding the new hybrid MPPSO, the flowchart of HMPPSO is showed in Fig. 2.

4.3. Validation of HMPPSO

Some well-known benchmark functions are used to test the performance of HMPPSO in this subsection. The basic information about them is listed in Table 1. In all experiments, if the object function is calculated more than 57600 times or the absolute fitness value of the present *gbest* comes to 0, the termination criteria meet. In SPSO and MPPSO, the swarm size is 30, and the maximum iteration is 1920 ($30 * 1920 = 57600$); In HMPPSO, every sub swarm size is 2 and iterates 4 times, the optimal swarm size is 8 and it iterates 4 times and repeats 4 times. The maximum iteration is 300 ($[2 * 8 * 4 + 8 * 4 * 4] * 300 = 57600$). The position of every particle is limited by the solution boundary of each function. The dimension of each function is set as $N = 30$ and $N = 50$. Each group of experiments independently go for 30 runs.

A series of items, including the best value, the worst value, the mean best value, the stand deviation and the average total object function evaluation time, are used to evaluate the HMPPSO and showed in related tables.

Table 2 and Fig. 3 show that HMPPSO can quickly converge to global minimum on the Griewank function while SPSO and MPPSO nearly stopped at anaphase. Fewer fitness function evaluation times are used and the final *gbest* particles are much closer to the theoretical global optimal. The mean fitness evaluation times are much less than

Table 1. Basic information about benchmark functions.

Function	Expression	min	Position scope	Velocity scope
Griewank	$f_3(x) = 1 + \frac{1}{4000}\sum_{i=1}^{N} x_i^2 - \prod_{i=1}^{N} \cos(\frac{x_i}{\sqrt{i}})$	0	[−600, 600]	[−100, 100]
Rosenbrock	$f_4(x) = \sum_{i=1}^{N-1}[100(x_{i+1} - x_i^2)^2 - (x_i - 1)^2]$	0	[−10, 10]	[−5, 5]

Table 2. Comparison on the Griewank function.

Algorithms	Dim (N)	Best value	Worst value	Mean value	Stand deviation	Average evaluation times
SPSO	30	0.01429	0.11476	0.04786	0.03051	57600
	50	0.48329	1.12681	0.94233	0.18307	57600
MPPSO	30	2.480e-8	5.880e-4	5.770e-5	1.123e-4	57600
	50	2.920e-8	5.240e-3	1.750e-4	2.753e-4	57600
HMPPSO	30	0	0	0	0	3929
	50	0	0	0	0	4826

Table 3. Comparison on the Rosenbrock function.

Algorithms	Dim (N)	Best value	Worst value	Mean value	Stand deviation	Average evaluation times
SPSO	30	19.9157	207.225	87.2424	48.7496	57600
	50	245.455	1571.55	450.748	242.979	57600
MPPSO	30	2.78231	11.2389	5.83943	2.1309	57600
	50	4.78185	45.5221	12.1417	7.1306	57600
HMPPSO	30	0.35738	4.42504	1.51337	1.00626	57600
	50	0.64860	5.99036	2.79761	1.60907	57600

57600 which indicates that it reaches the global optimal for most of times. For the Rosenbrock function in Table 3 and Fig. 4, it is clear that the MPPSO can find the smallest fitness function value with the same fitness function evaluation times. Besides, with the increase of the dimensions, the best value of HMPPSO changes little, while MPPSO and SPSO change much more.

According to the Tables 2, 3 above, the results of HMPPSO are

much closer to the theoretical optima, and HMPPSO is superior to PSO and SPSO in terms of such items as the best value, the worst value, the mean best value and the stand deviation. From Figs. 3, 4, it can be seen that the dynamic curves of mean fitness values using HMPPSO decrease much faster and much lower by than those using SPSO and MPPSO. So the conclusion is that HMPPSO is more efficient and robust than both SPSO and MPPSO.

5. SIMULATION RESULTS

In order to show the efficiency and effectiveness of the proposed HMPPSO for through-wall metallic cylinder shape reconstruction and wall parameters estimation, some numerical results are presented in this section. In all the numerical simulations, the scattered fields are computed following Equation (1) along the 3 m-long measurement line with step of 15 cm (i.e., N_y= 21) posited at $x_A = -1.0$ m at three different frequencies (i.e., $N_f = 3$): 1, 1.5 and 2 GHz. Generally, the data are always contaminated by the noise in real measurement; therefore, some additive Gaussian white noise following a normal distribution with mean zero and standard deviation σ^2_{noise} is added to the calculated data as follow [19]:

$$SNR = 10\log_{10}\frac{\sum_{m=1}^{N_f}\sum_{n=1}^{N_y}\left|E_z^r\left(y_n,k_m\right)\right|^2}{2N_fN_y\sigma^2_{noise}}\ (\text{dB}) \tag{11}$$

Here SNR is signal noise ratio, in this paper, $N_f = 3$, $N_y = 21$, $SNR = 20$. For HMPPSO, each sub swarm iterates 4 times and its size is 2, the optimal swarm size is 8 and iterates 4 times, and it will repeat for 4 times. When the maximum iteration comes to 150 or the cost function reaches 0.001, the HMPPSO is stopped.

Firstly, the reconstruction of a circular metallic cylinder behind a single layer homogenous wall is presented. Suppose that the wall thickness $d = 0.3$ m, conductivity $\sigma = 0.01$ S/m, the relative dielectric permittivity $\epsilon_r = 5.0$ and the radius of the circular metallic cylinder, which posited at $x_S = -2.3$ m, is $R = 0.3$ m. The particle size is 4, corresponding to the 4 parameters (d, σ, ϵ_r and the radius of the circular metallic cylinder R) to be reconstructed, each of which is limited by the solution boundary shown in Table 4. In the following tables, R.V. represents the reconstructed value, R.E. represents the relative error.

The 4 parameters are reconstructed simultaneously and their results are shown in Table 4. It can be seen that without the noise, the true values and reconstructed ones are much the same, with all the relative errors less than 4.0%. With 20 dB additive Gaussian white noise added to the scattering data, the errors are larger, but still less

Table 4. The boundaries and the reconstruction results by HMPPSO.

Parameter	Searching boundary	True value	R.V. (noiseless)
R (m)	[0.1, 0.5]	0.3	0.3114
d (m)	[0.1, 0.5]	0.3	0.3052
ϵ_r	[2.0, 8.0]	5.0	4.9642
σ	[0.001, 0.1]	0.01	0.0096
Parameter	R.E. (noiseless)	R.V. (20 dB)	R.E. (20 dB)
R (m)	3.80%	0.2865	4.50%
d (m)	1.73%	0.3147	4.90%
ϵ_r	0.80%	5.1542	3.08%
σ	4.00%	0.01067	6.70%

than 7% (most below 5%). To some extent, it can be said that the parameters are truly reconstructed even with the noise.

Then, the reconstruction of a metallic cylinder with the cross section of any irregular continuous shape behind a single layer homogenous wall is presented. Suppose that the cylinder shape is represented by trigonometric series as: $r'(\phi') = 0.25 + 0.1\cos(2\phi') + 0.1\sin(2\phi')$. The other wall parameters are the same as the above numerical simulation. When the HMPPSO is used for this reconstruction, the particle size is 10, corresponding to the 10 parameters to be reconstructed. They are reconstructed simultaneously and their results are shown in Table 5 and Fig. 6.

From Table 5, it can be seen that without the noise, the reconstructed wall and shape parameters are quite satisfactory because they are very close to the true values and, with almost all the relative error around 2.0%. With 20 dB additive Gaussian white noise added to the scattering data, the relative errors are larger, but they are still acceptable, because they are all less than 8% (most around 5%). To some extent, we can say that the unknown parameters are successfully reconstructed even with the noise. The reconstructed shapes are shown in Fig. 5. From Fig. 5(a), while the reconstructed shape with noiseless data is quite close to the true shape, the difference between the true shape and the reconstructed one with 20 dB noise is bigger, but they still agree. To make a comparison with HMPPSO, simulations by PSO on the same shape with the same fitness evaluation times (30 particles, 960 iterations) are also provided. It is obviously from the figure that the shapes reconstructed by HMPPSO are much closer to

Table 5. The boundaries and reconstruction results of the first shape by HMPPSO.

Parameter	Searching boundary	True value	R.V. (noiseless)
d (m)	$[0.1, 0.5]$	0.30	0.3016
ϵ_r	$[2.0, 8.0]$	5.0	4.928
σ	$[0.001, 0.1]$	0.01	0.009465
a_0 (m)	$[0.0, 0.5]$	0.25	0.2522
a_1 (m)	$[-0.1, 0.3]$	0.0	0.001959
a_2 (m)	$[-0.1, 0.3]$	0.1	0.1001
a_3 (m)	$[-0.1, 0.1]$	0.0	-0.001269
b_1 (m)	$[-0.1, 0.1]$	0.0	0.0004031
b_2 (m)	$[-0.1, 0.3]$	0.1	0.09732
b_3 (m)	$[-0.1, 0.1]$	0.0	-0.002266
Parameter	R.E. (noiseless)	R.V. (20 dB)	R.E. (20 dB)
d (m)	0.62%	0.2835	5.51%
ϵ_r	1.45%	5.262	5.24%
σ	5.35%	0.01074	7.42%
a_0 (m)	0.86%	0.2586	3.42%
a_1 (m)	–	0.006554	–
a_2 (m)	0.14%	0.09459	5.41%
a_3 (m)	–	-0.003497	–
b_1 (m)	–	-0.005742	–
b_2 (m)	2.68%	0.09696	3.04%
b_3 (m)	–	-0.001664	–

the true shape. In Fig. 5(b), the cost function drops very quickly at the anaphase, which is similar to the simulations on the benchmarks functions as above. Besides, the cost function without noise is smaller than that with noise, and it is smaller by HMPPSO than by PSO. Smaller cost function corresponds to more accurate reconstruction result, which is in accordance with what shows in Table 5 and Fig. 5(a). As depicted above, it is concluded that the HMPPSO is much better than PSO and it is noise-tolerance to some extent when used in through wall shape reconstruction and wall parameter estimation.

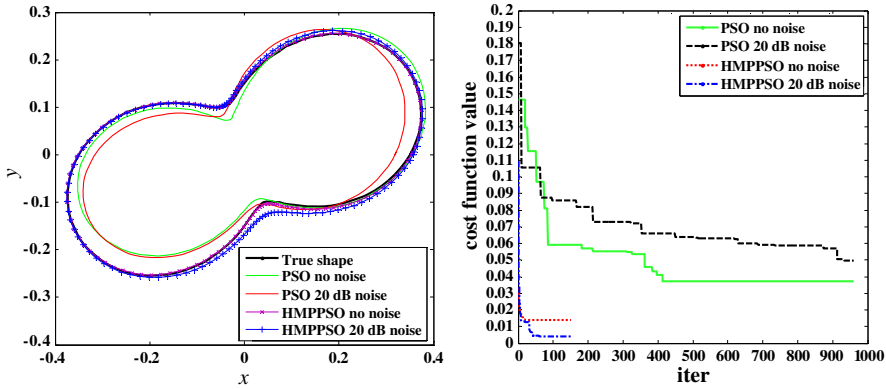

Figure 5. The first shape reconstruction by HMPPSO. (a) Reconstructed shapes, (b) cost function value with iterations.

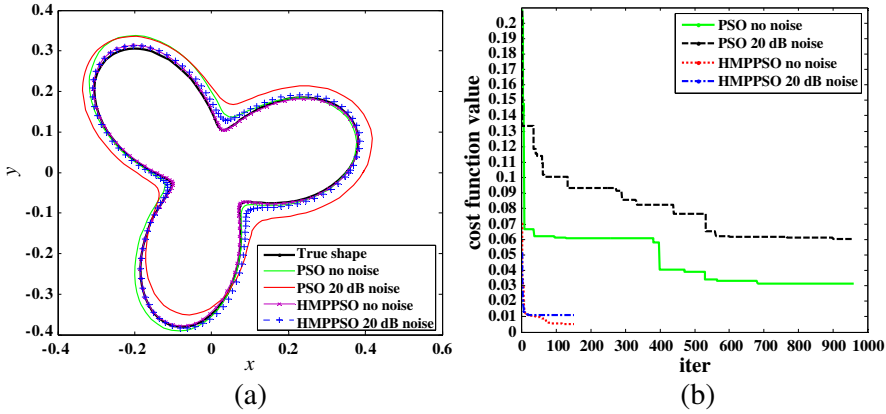

Figure 6. The second shape reconstruction by HMPPSO. (a) Reconstructed shapes, (b) cost function value with iterations.

To show the flexibility of the HMPPSO in irregular shape reconstruction, another example is shown. Suppose that the cylinder shape is represented as: $r'(\phi') = 0.25 + 0.1\cos(3\phi') + 0.1\sin(3\phi')$. The other wall parameters are all the same with the above simulation. All the 10 parameters are reconstructed simultaneously and the results are illustrated in Table 6 and Fig. 6.

The information in Table 6 and Fig. 6 is quite the same with that in Table 5 and Fig. 5, so their conclusions are the same. So we do not decide to repeat them here.

Table 6. The boundaries and reconstruction results of the second shape by HMPPSO.

Parameter	Searching boundary	True value	R.V. (noiseless)
d (m)	[0.1, 0.5]	0.30	0.3010
ϵ_r	[2.0, 8.0]	5.0	4.969
σ	$[0.001, 0.1]$	0.01	0.01047
a_0 (m)	[0.0, 0.5]	0.25	0.2495
a_1 (m)	$[-0.1, 0.1]$	0.0	-6.41e-005
a_2 (m)	$[-0.1, 0.1]$	0.0	-0.001050
a_3 (m)	$[-0.1, 0.3]$	0.1	0.1046
b_1 (m)	$[-0.1, 0.1]$	0.0	0.003235
b_2 (m)	$[-0.1, 0.1]$	0.0	-0.002455
b_3 (m)	$[-0.1, 0.3]$	0.1	0.09770
Parameter	R.E. (noiseless)	R.V. (20 dB)	R.E. (20 dB)
d (m)	0.34%	0.3042	1.40%
ϵ_r	0.63%	4.802	3.95%
σ	4.68%	0.009313	8.42%
a_0 (m)	0.20%	0.2619	4.76%
a_1 (m)	–	0.005212	–
a_2 (m)	–	-0.003690	–
a_3 (m)	4.58%	0.09279	7.2%
b_1 (m)	–	0.002459	–
b_2 (m)	–	-0.003967	–
b_3 (m)	2.30%	0.09514	4.86%

6. CONCLUSION

In this study, a hybrid multi-phased particle swarm optimization algorithm (HMPPSO) is proposed for 2D through-wall metallic cylinder shape reconstruction and wall parameters estimation. By adopting the small swarm size strategy and the idea of "sub swarms" working cooperatively and alternatively with "optimal swarm", the HMPPSO can converge quickly with much less forward scattering problem solving times, thus reduces the reconstruction time. The forward problem is computed using the method of moments. The

inverse problem is reformulated in to an optimization one, and then the global searching scheme HMPPSO is employed to reconstruct the unknowns from simulated data. Numerical results shows that the wall parameters together with target shape parameters with 20 dB additive Gaussian white noise are successfully reconstructed by HMPPSO algorithm. Future work will involve evaluating the algorithm on 3D dielectric simulations and using real measured data.

ACKNOWLEDGMENT

This work was supported by the National Key Laboratory of Millimeter Waves at Southeast University in China (No. K201201); the Natural Science Foundation of Shaanxi Province, China (No. 2011JM8025).

REFERENCES

1. Qing, A. and L. Jen, "A novel method for microwave imaging of dielectric cylinder in layered media," *Journal of Electromagnetic Waves and Applications*, Vol. 11, No. 10, 1337–1348, 1997.
2. Huang, Q., L. L. Qu, B. H. Wu, and G. Y. Fang, "UWB through-wall imaging based on compressive sensing," *IEEE Trans. on Geosci. Remote Sens.*, Vol. 48, No. 3, 1408–1415, 2010.
3. Caorsi, S., A. Massa, and M. Pastrorino, "Iterative numerical computation of the electromagnetic fields inside weakly nonlinear infinite dielectric cylinders of arbitrary cross section using distorted-wave born approximation," *IEEE Transactions on Microwave Theory and Techniques*, Vol. 44, No. 3, 400–412, 1996.
4. Abubakar, A. and P. M. van den Berg, "The contrast source inversion method for location and shape reconstructions," *Inverse Problems*, Vol. 18, 495–510, 2002.
5. Chen, X. D., "Subspace-based optimization method for solving inverse-scattering problems," *IEEE Trans. on Geosci. Remote Sens.*, Vol. 48, No. 3, 42–49, 2010.
6. Kirsch, A., "The MUSIC-algorithm and the factorization method in inverse scattering theory for inhomogeneous media," *Inverse Problems*, Vol. 18, 1025–1040, 2002.
7. Kidera, S., T. Sakamoto, and T. Sato, "High-resolution 3-D imaging algorithm with an envelope of modified spheres for UWB through-the-wall radars," *IEEE Transactions on Antennas and Propagation*, Vol. 57, No. 11, 3520–3529, Nov. 2009.
8. Van den Berg, P. M. and M. van der Horst, "Nonlinear inversion

in induction logging using the modified gradient method," *Radio Sci.*, Vol. 30, 1355–1369, 1995.

9. Hettlich, F., "Two methods for solving an inverse conductive scattering problem," *Inverse Problems*, Vol. 10, 375–385, 1994.
10. Rekanos, I. T., "Shape reconstruction of a perfectly conducting scatter using differential evolution and particle swarm optimization," *IEEE Trans. on Geosci. Remote Sens.*, Vol. 46, No. 7, 1967–1974, 2008.
11. Qing, A., C. K. Lee, and L. Jen, "Electromagnetic inverse scattering of two-dimensional perfectly conducting objects by real-coded genetic algorithm," *IEEE Trans. on Geosci. Remote Sens.*, Vol. 39, No. 3, 665–676, 2001.
12. Dehmollaian, M., "Through-wall shape reconstruction and wall parameters estimation using differential evolution," *IEEE Geosciences and Remote Sensing Letters*, Vol. 8, No. 2, 201–205, 2011.
13. Brignone, M., G. Bozza, A. Randazzo, M. Piana, and M. Pastorino, "A hybrid approach to 3D microwave imaging by using linear sampling and ACO," *IEEE Transactions on Antennas and Propagation*, Vol. 56, No. 10, 3224–3232, 2008.
14. Kennedy, J. and R. C. Eberhart, *Swarm Intelligence*, Morgan Kaufmann, San Francisco, 2001.
15. Huang, T. and A. Sanagavarapu, "A microparticle swarm optimizer for the reconstruction of microwave images," *IEEE Transactions on Antennas and Propagation*, Vol. 55, No. 3, 568–576, 2007.
16. Mhamdi, B., K. Grayaa, and T. Aguili, "Hybrid of particle swarm optimization, simulated annealing and tabu search for the reconstruction of two-dimensional targets from laboratory-controlled data," *Progress In Electromagnetics Research B*, Vol. 28, 1–18, 2011.
17. Huang, C.-H., C.-C. Chiu, C.-L. Li, and K.-C. Chen, "Time domain inverse scattering of a two-dimensional homogenous dielectric object with arbitrary shape by particle swarm optimization," *Progress In Electromagnetics Research*, Vol. 82, 381–400, 2008.
18. Donelli, M. and A. Massa, "Computational approach based on a particle swarm optimization for microwave imaging of two dimensional dielectric scatters," *IEEE Transactions on Microwave Theory and Techniques*, Vol. 53, No. 5, 1761–1776, 2005.
19. Donelli, M., D. Franceschini, P. Rocca, and A. Massa, "Three

dimensional microwave imaging problems solved through an efficient multiscaling particle swarm optimization," *IEEE Trans. on Geosci. Remote Sens.*, Vol. 47, No. 5, 1467–1481, 2009.

20. Emad Eldin, A. M., E. A. H. Hashish, and M. I. Hassan, "Inversion of lossy dielectric profiles using particle swarm optimization," *Progress In Electromagnetics Research M*, Vol. 9, 93–105, 2009.
21. Al-kazemi, B. S. N., "Multi-phase particle swarm optimization," Syracuse University, May 2002.
22. Al-Kazemi, B. and C. K. Mohan, "Muti-phase discrete particle swarm optimization," *Proc. the Fourth International Workshop on Frontiers in Evolutionary Algorithms*, 2000.
23. Jie, J., J. C. Zeng, and C. Z. Han, "Knowledge based cooperative particle swarm optimization," *Applied Mathematics and Computation*, Vol. 205, No. 2, 861–873, 2008.